Environmental Science & Technology

pubs.acs.org/est

Article

Biological Oxidation of Fe(II)-Bearing Smectite by Microaerophilic Iron Oxidizer *Sideroxydans lithotrophicus* Using Dual Mto and Cyc2 Iron Oxidation Pathways

Nanqing Zhou, Robert J. Kupper, Jeffrey G. Catalano, Aaron Thompson, and Clara S. Chan*

Cite This: https://doi.org/10.1021/acs.est.2c05142

Read Online

ACCESS | Metrics & More | Article Recommendations | Supporting Information

ABSTRACT: Fe(II) clays are common across many environments, making them a potentially significant microbial substrate, yet clays are not well established as an electron donor. Therefore, we explored whether Fe(II)-smectite supports the growth of *Sideroxydans lithotrophicus* ES-1, a microaerophilic Fe(II)-oxidizing bacterium (FeOB), using synthesized trioctahedral Fe(II)-smectite and 2% oxygen. *S. lithotrophicus* grew substantially and can oxidize Fe(II)-smectite to a higher extent than abiotic oxidation, based on X-ray near-edge spectroscopy (XANES). Sequential extraction showed that edge-Fe(II) is oxidized before interior-Fe(II) in both biotic and abiotic experiments. The resulting Fe(III) remains in smectite, as secondary minerals were not detected in biotic and abiotic oxidation products by XANES and Mössbauer spectroscopy. To determine the genes involved, we compared *S. lithotrophicus* grown on smectite versus Fe(II)-citrate using reverse-transcription quantitative PCR and found that *cyc2* genes were highly expressed on both substrates, while *mtoA* was upregulated on smectite. Proteomics confirmed that Mto proteins were only expressed on smectite, indicating that ES-1 uses the Mto pathway to access solid Fe(II). We integrate our results into a biochemical and mineralogical model of microbial smectite oxidation. This work increases the known substrates for FeOB growth and expands the mechanisms of Fe(II)-smectite alteration in the environment.

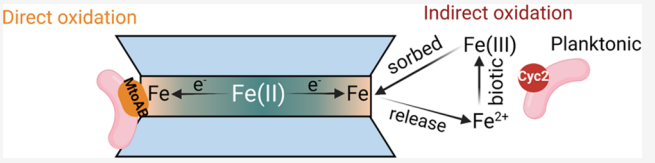

KEYWORDS: *smectite, clay, Fe(II) oxidation, Fe(II)-oxidizing bacteria, extracellular electron transport*

INTRODUCTION

Iron (Fe) is abundant in the Earth's crust, occurring mostly in the solid phase in mineral structures. Smectite is a common 2:1 clay mineral[1] that can contain substantial Fe and play important roles in contaminant degradation,[2−4] heavy metal immobilization,[5−7] and nutrient cycling.[8] Trioctahedral Fe(II)-smectite, a major product of basalt alteration,[9,10] is widespread in the ocean crust,[11−13] as well as other subsurface terrestrial and marine settings,[14−16] forming a large electron pool that may support neutrophilic Fe(II)-oxidizing bacteria (FeOB) growth.

Most FeOB cultivation uses aqueous Fe(II),[17−19] so it is unclear if FeOB can grow on solid Fe(II), including smectite. Fe(II) clays can be oxidized by heterotrophic nitrate-reducing bacteria.[20−22] However, these studies used nitrate-reducing bacteria that largely rely on organic substrates, producing nitrite that can abiotically oxidize Fe(II), including in clay,[23−25] so it is unclear to what extent Fe oxidation supports growth. In contrast, the Fe(II) phyllosilicate biotite has been shown to support chemolithotrophic growth of the nitrate-reducing, Fe(II)-oxidizing culture KS.[26] The fact that biotite and smectite are both 2:1 sheet silicates suggests that FeOB growth on smectite clays should also be possible.

To grow on Fe(II)-smectite, microbes need mechanisms to be able to uptake electrons from the solid electron source. Previous studies have proposed two potential pathways for microbial Fe(II) oxidation: Cyc2 and MtoAB/PioAB pathways.[27−30] Cyc2 is used in oxidizing dissolved Fe(II), as demonstrated in our study on the microaerophilic FeOB *Sideroxydans lithotrophicus* ES-1.[31] Genes for MtoAB were expressed at a very low level and not responsive to Fe(II)-citrate.[31] MtoAB is hypothesized to be used to interact with solid Fe(II), similar to the interaction of the homologous MtrAB(C) with Fe(III) minerals. As a sparingly soluble Fe(II) mineral, smectite can be used to reveal the mechanisms of solid Fe(II) oxidation.

Microbial interactions with smectite depend on the mineral structure and reactivity, so we need to carefully choose the substrate and track Fe(II)/Fe(III). The most commonly used Fe clay in microbial experiments is the nontronite NAu-2,[20−22,32,33] a natural Fe(III) clay standard. To test microbial oxidation, previous studies have reduced Fe(III) in NAu-2 to Fe(II) chemically or microbially.[20−22] The reduced Fe(II) remains in the NAu-2 dioctahedral structure, with variable

Received: July 18, 2022
Revised: October 3, 2022
Accepted: October 24, 2022

distribution.[34,35] In contrast, native Fe(II)-smectites are trioctahedral, and this structural difference could cause variation in reactivity, which depends on the distribution of Fe in the structure. However, trioctahedral smectite is generally unavailable for experimentation because of its sensitivity to oxygen.[36] Studies of dioctahedral smectites show that edge-Fe is more reactive,[35,37] but interior-Fe within the crystal lattice could be accessible via electron hopping between Fe.[35,38−43] To track microbial usage of smectite Fe, it is necessary to monitor different Fe fractions. This will tell us whether Fe(II) in smectite is dissolved and subsequently oxidized to form secondary minerals or if Fe(III) is retained in smectite. This monitoring will also show whether microbes can use interior-Fe, which will control the extent to which microbes can grow on smectite.

In this study, we investigated *S. lithotrophicus* ES-1, a type strain of the widely distributed Fe-oxidizing genus *Sideroxydans*.[44−49] Importantly, ES-1 has genes that encode both Cyc2 and MtoAB,[27,28] which enables us to differentiate the functions of the two pathways in oxidizing aqueous and solid Fe(II) using the same microbe. In this work, we tested ES-1 growth on chemically synthesized trioctahedral Fe(II)-smectite, characterized the products, and demonstrated the distinct roles of Cyc2 and MtoAB in microbial Fe oxidation. These results help us to better understand how clay minerals support life and how microbes drive Fe redox reactions that impact fates of contaminants, heavy metals, and nutrients.

MATERIAL AND METHODS

Biotic and Abiotic Smectite Oxidation. The Fe(II)-smectite was synthesized using an established sol−gel method[50] with a modification to maintain anaerobic conditions during hydrothermal treatment.[51] The chemical formula of the synthesized trioctahedral smectite with low vacancies is $Ca_{0.17}(Fe_{1.71}^{II}Al_{0.35}Mg_{0.78})(Si_{3.60}Al_{0.40})O_{10}(OH)_2$. The ratio of Fe/Mg/Al in the mineral is 53:24:23, which is a representative of natural trioctahedral Fe(II)-bearing smectites.[14,16,52−55] ES-1 cells were cultured in modified Wolfe's minimal medium (MWMM) buffered with 20 mM 2-(*N*-morpholino)-ethanesulfonic acid (MES) and adjusted to pH 6.0. Trioctahedral Fe(II)-rich smectite (1 g/L) was added into the culture as the electron donor. The headspace was filled with 78% N_2/20% CO_2/2% O_2 gas mix and refreshed every day with a slight overpressure in the bottles. Triplicate setups of small batch cultures were prepared to monitor cell growth and Fe consumption. The setups included cell and smectite, cell-free and smectite-free incubations. To acquire a sufficient amount of mineral products for characterization, cultures were scaled up to 250 mL. The cell number was recorded by direct cell counting using fluorescence microscopy after staining the cells with Syto13 in a Hausser counting chamber.

Fe Species Analysis from Small Batch Cultures. The consumption of different solid Fe(II) species can be tracked by sequential extraction in three steps: (i) $CaCl_2$ extraction to remove basal plane-Fe(II), (ii) NaH_2PO_4 extraction to release Fe(II) bound to the edge sites as well as reactive interior-Fe(II),[42] and (iii) ammonium hydrogen fluoride (NH_4HF_2) dissolution of less-reactive interior-Fe(II). At selected time points, 1.5 mL of culture suspension was taken using a syringe and needle in the anaerobic glove box and filtered through a 13 mm PTFE membrane (0.22 μm). The filtrate was collected to measure the aqueous Fe(II), and the filter membrane material was resuspended in 1.5 mL of 1 M $CaCl_2$ (pH 7) for 4 h to extract the Fe(II) sorbed on the basal plane. Then, the suspension was centrifuged at 16,000 *g* for 2 min to collect the supernatant. The remaining solids were washed once with deoxygenated DI water and extracted with 1.5 mL of 1 M NaH_2PO_4 (pH 5) for 18 h to isolate the Fe(II) associated with the edge OH-groups.[42] After the phosphate extraction, the remaining solids were dissolved in 1.5 mL of 20 g/L NH_4HF_2. All centrifugation and washing steps were performed under anoxic conditions. Fe(II) was measured by a 1,10-phenanthroline assay. The total Fe concentration was determined by adding 10% hydroxylamine-HCl to reduce Fe(III) in the samples, followed by the 1,10-phenanthroline assay.[56]

TEM. Transmission electron microscopy (TEM) was carried out on the late-log phase smectite culture using a Zeiss LIBRA 120 transmission electron microscope operating at 200 kV. The samples were deposited onto a lacey carbon-coated copper grid and washed twice with one drop of nanopure water after sitting for 30 min. The sample grid was air-dried before imaging.

Mineral Collection from Scaled-Up Cultures. Biotic and abiotic mineral samples were harvested from 250 mL cultures to perform Fe K-edge X-ray absorption spectroscopy and Mössbauer spectroscopy on day 2 and day 7 to represent the mid-log and late-log growth phases, respectively. The mineral products were harvested by centrifuging at 4000 *g* for 10 min and washed three times using deoxygenated water. The samples were dried in a desiccator in the anaerobic chamber.

^{57}Fe Mossbauer Spectroscopy (MBS) Data Collection and Fitting. The mineral solids were mixed with boron nitride and ground into a fine powder using an agate mortar and pestle. Then, the sample powder was sealed in two pieces of Kapton tape in an anaerobic chamber and sent for Mössbauer spectroscopy at the University of Georgia. Transmission ^{57}Fe Mössbauer absorption spectra were collected under three temperatures (295, 13, 5 K) with a He-cooled system and a 1024 channel detector. ^{57}Fe Mössbauer spectroscopy data collected under 295 and 13 K were fitted using the Voigt-based fitting method of Rancourt and Ping[57] with the Recoil software. All fitting and calculated parameters are as defined by Rancourt and Ping.[57] Additional details are given in the SI section 2.

X-ray Absorption Spectroscopy (XAS). Fe K-edge X-ray absorption spectroscopy was performed to determine the oxidation state of Fe in the smectite and identify mineralogical changes in the smectite after biotic and abiotic oxidation. XAS was conducted at beamlines 12-BM-B at the Advanced Photon Source at Argonne National Laboratory. Transmission measurements were made for the samples, with the energy selected using a Si (111) fixed-offset monochromator. The harmonic content of the beam was minimized by detuning the second monochromator crystal by 20% and by insertion of toroidal and flat X-ray mirrors.

The raw spectral scans were averaged and normalized using Athena,[58] and iron oxidation states were quantified via linear combination fitting (LCF) of the X-ray absorption near-edge structure (XANES) using a series of smectite standards. The standards include the unaltered trioctahedral smectite, nontronite (NAu-2), and peroxide-treated smectite since peroxide has been reported to completely oxidize Fe(II)-smectite.[59] The EXAFS spectra were k^3-weighted and fitted to a local structural model using Artemis.[58] Scattering paths for EXAFS fitting were generated from the siderophyllite structure[60] with H removed using FEFF6.[61] Only single scattering paths in the first and

https://doi.org/10.1021/acs.est.2c05142
Environ. Sci. Technol. XXXX, XXX, XXX−XXX

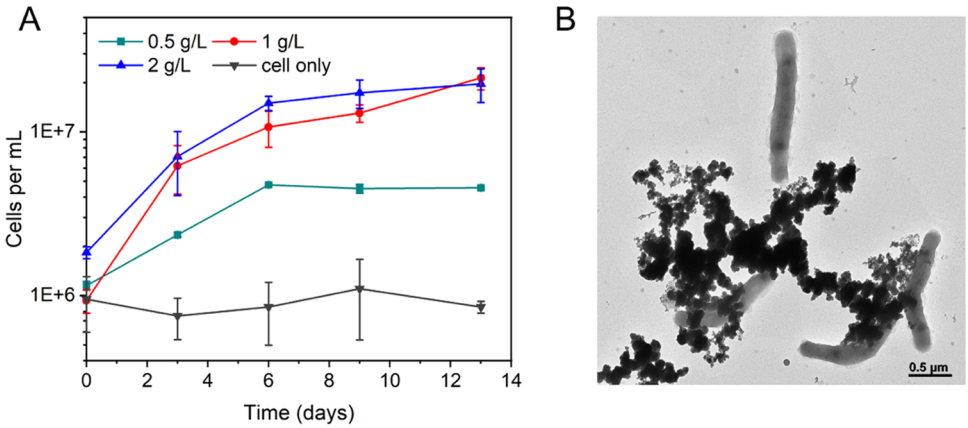

Figure 1. (A) Growth curve of ES-1 on different concentrations of Fe(II)-smectite. The error bars represent the standard error of triplicates. (B) TEM image of ES-1 in smectite culture at the late-log growth phase. More TEM images are shown in Figure S1.

second shells were considered. For each scattering path, the amplitude reduction factor (S_0^2) was set as 0.9, while the interatomic distance (R); the coordination numbers (N) for Fe−Fe, Fe−Mg, and Fe−Al; and a Debye−Waller factor representing disorder (σ^2) were determined using nonlinear least-squares fitting. The coordination numbers of Fe−O and Fe−Si were set as 6 and 4, respectively, and relative values of N for Fe−Fe, Fe−Mg, and Fe−Al were held in proportion based on the stoichiometry in the smectite formula.

Experimental Setup for RNA Extraction from Scaled-Up Cultures. To compare the different mechanisms ES-1 uses to oxidize solid and aqueous Fe(II), smectite and Fe(II)-citrate were provided as the electron donors. Smectite was added once (at the time of inoculation) to reach a concentration of 1 g/L, while Fe(II)-citrate was amended daily to reach a target concentration of 500 μM. Cells were harvested at the mid-log phase (day 2) and late-log phase (day 5 for Fe(II)-citrate culture and day 7 for smectite culture) by filtering through a 0.22-micron membrane (Millipore GTTP). In addition, an Fe(II)-source switch experiment was performed to further investigate if the substrate change induces changes in gene expression in response to different Fe(II) sources. When the cells reached the late-log phase, the Fe(II) source was switched by inoculating smectite-grown cells into fresh media supplied with Fe(II)-citrate and vice versa (details are provided in the SI). Cells were harvested when they reached the mid-log phase after the Fe(II) source switch. RNA was extracted from the cells collected on the filter membrane using Qiagen RNeasy Micro kit as previously described.[31]

Reverse-Transcription Quantitative PCR (RT-qPCR). Total RNA (0.5 ng) was input as a template to synthesize cDNA using the Maxima First Strand cDNA Synthesis Kit (Thermo Scientific). Gene expression of three *cyc2* genes and *mtoA* was quantified with *gyrB* as the reference gene. Primers designed for the target genes were adopted from our previous study.[31] Quantabio SYBR Green supermix and the Bio-Rad CFX96 Real-Time PCR system were used to perform the quantification assays using the program from our previous study.[31] Each biological replicate was run in two technical replicates.

Proteomics. *Protein Extraction.* To obtain a sufficient amount of biomass for proteomics, we combined four 250 mL ES-1 cultures grown on either smectite or Fe(II)-citrate and collected at the late-log phase by filtration through a 0.22 μm membrane (Millipore GPWP). Each growth condition was sampled in triplicate. Then, the membranes were cut into small pieces and vortexed with lysing matrix E and 2 mL of lysis buffer, which is composed of 100 mM Tris/HCl, 10 mM ethylenediaminetetraacetic acid (EDTA), pH 8.0, 0.05% Tween-20, and 1% w/v sodium dodecyl sulfate (SDS). After vortexing, the cell lysate was centrifuged at 14,000 *g* for 10 min. The supernatant was collected and concentrated using a 10 kDa spin concentrator (Millipore). Then, the protein concentration was determined by a fluorescence assay using the Qubit protein BR assay kit. The lysates were then digested, desalted, and analyzed in the Mass Spectrometry Core at the University of Delaware. Detailed information on the digestion, desalting, and mass spec analysis processes is provided in the SI.

Data Processing and Protein Quantification. The protein database of*S. lithotrophicus*ES-1 was downloaded from Uniprot (www.uniprot.org). MaxQuant v1.6.3.4 was used for protein quantification, and the false discovery rate (FDR) of less than 1% was required.[62] Filtering, bioinformatics, and statistical analyses of the MaxQuant output were performed in Perseus v1.6.15.0.[63] The label-free quantitation (LFQ) intensities were log (base 2) transformed, and the missing values were replaced by applying a normal distribution downshift using the Perseus default setting. To identify the differentially expressed proteins, a two-sample *t*-test was performed with the cutoff p-value less than or equal to 0.05. The raw proteome data file was deposited to MassIVE with an accession number of MSV000089149.

RESULTS

ES-1 Growth on Smectite and the Biological Consumption of Different Fe(II) Species. Different concentrations of smectite were added to 80 mL ES-1 culture to investigate whether ES-1 can grow on Fe(II)-smectite and if smectite concentration influences the biomass yield. No cell growth was observed in the smectite-free culture. The ES-1 cell number increased 4.7 fold as the smectite concentration increased from 0.5 to 1 g/L, suggesting ES-1 used smectite as the substrate to grow (Figure 1A). The maximum cell number was around 2.1×10^7 cells per mL, which is comparable to the maximum cell number we have observed in aqueous Fe(II) culture.[31] Increasing the smectite concentration to 2 g/L did not lead to higher cell density; therefore, a smectite concentration of 1 g/L was chosen for the further experiments. TEM imaging from air-dried samples shows that the smectite

https://doi.org/10.1021/acs.est.2c05142
Environ. Sci. Technol. XXXX, XXX, XXX−XXX

mineral particles are nanosized (Figures 1B and S1), which provides a large surface area to interact with microbes. Cells are straight or curved rods, and no outer-membrane extensions were observed in the TEM images.

Many Fe(II)-bearing minerals have been found to release dissolved Fe(II) into solution,[64−66] which can support FeOB growth together with the mineral-associated Fe(II). The presence of different Fe(II) sources could confound interpretations of the oxidation pathway since microbes might use different pathways to access the solid and aqueous Fe(II). To test if Fe(II)-smectite releases aqueous Fe(II), the dissolved Fe(II) concentrations were measured in MWMM media with 1 g/L of smectite in the absence of oxygen. Smectite released Fe(II) rapidly initially; then, the release rate slowed down and ceased after 6 days (Figure S2A). The final dissolved Fe(II) concentration was ∼80 μM in the 1 g/L smectite culture (Figure S2A) without constant dissolution, which accounts for ∼2% of the total Fe(II). To test if the dissolved Fe(II) is the main source supporting ES-1 growth, we compared ES-1 cell density in 1 g/L of smectite culture with a daily supply of 100 μM aqueous Fe(II) culture. Fe(II) monitoring showed that aqueous Fe(II) was completely consumed during incubation before another feeding, so there was no Fe(II) accumulation. The final cell density in the smectite culture was one magnitude higher than that in the aqueous Fe(II) culture (Figure S2B), suggesting that ES-1 growth on dissolved Fe(II) could not account for the cell yields in the smectite culture, so we conclude that cells mainly grow on the solid Fe(II) in the smectite structure.

Fe(II)-smectite contains three solid Fe(II) species: basal plane-Fe(II), edge-Fe(II), and interior-Fe(II).[35,37] Our data show that the $CaCl_2$-extractable basal plane-Fe(II) only accounts for a small proportion of Fe(II) in smectite (1−5%) (Figure 2), which is consistent with the proportion in

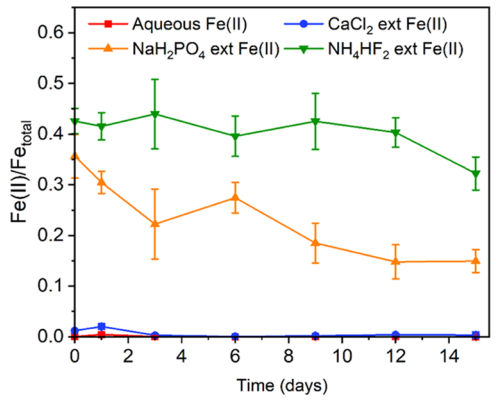

Figure 2. Proportion change of different Fe(II) fractions during a 15-day incubation with ES-1. The abiotic oxidation of different Fe(II) fractions is shown in Figure S3.

reduced nontronite.[42] The NaH_2PO_4-extractable reactive Fe(II) and NH_4HF_2-dissolved less-reactive interior-Fe(II) are the major Fe(II) fractions in the unaltered smectite (Figure 2). During the incubation, the proportion of reactive NaH_2PO_4-extractable Fe(II) decreased quickly after inoculation, while the less-reactive interior-Fe(II) remained unchanged until day 12 (Figure 2). Therefore, ES-1 preferentially oxidized the more reactive Fe(II), especially the edge-Fe(II) in the smectite structure, which is consistent with previous reports on biotic smectite reduction and oxidation.[22,67] After day 12, the NaH_2PO_4-extractable Fe(II) ceased decreasing and the less-reactive interior-Fe(II) began to decrease, suggesting that the interior-Fe(II) was used by the cells, despite the fact that cells cannot directly contact the interior-Fe(II).

Comparison of Biotic and Abiotic Smectite Oxidation. Biotic oxidation of aqueous Fe(II) has been demonstrated to outcompete abiotic oxidation at low oxygen levels,[68,69] but it is unclear if that is also true for Fe(II) mineral oxidation. Therefore, $Fe(II)/Fe_{total}$ changes were monitored and compared between biotic and abiotic oxidation in a small batch (80 mL), initially using a phenanthroline assay. By this method, the mean values of $Fe(II)/Fe_{total}$ in the biotic group were lower than the values in the abiotic group at most of our sample time points, but the difference was not significant due to the data scatter, with the exception of the last data point on day 15 ($p < 0.05$, t-test) (Figure 3A). We then compared the biotic and abiotic oxidation rates and extents of the two major Fe(II) fractions: reactive NaH_2PO_4-extractable Fe(II) and less-reactive interior-Fe(II) dissolved by NH_4HF_2. There was no significant difference between biotic and abiotic consumption of NaH_2PO_4-extractable Fe(II) and less-reactive NH_4HF_2-extracted Fe(II) ($p > 0.05$, t-test), though there appears to be more biotic oxidation of NH_4HF_2-extracted Fe(II) at 15 days. Overall, based on these phenanthroline assay results, it is inconclusive if microbes catalyze Fe(II)-smectite oxidation at a different rate or extent than strictly abiotic processes.

Fe K-edge XANES and MBS were better able to resolve the difference in oxidation extent between bulk biotic and abiotic products. These products were collected from a scaled-up batch (250 mL) with the same synthesized smectite to obtain sufficient amounts of minerals on days 2 and 7, which correspond to ES-1 mid-log and late-log growth phases. XANES data for samples collected on day 7 showed a higher oxidation extent than the day 2 samples (Figure 4A), given the higher Fe K-edge positions in day 7 samples. On day 7, the XANES LCF showed that the biotic oxidation product had less Fe(II) (62.3 ± 1.0%) than the abiotic oxidation product (80.3 ± 1.4%) (Figure 4B and Table S1). MBS fitting at 295 K agrees with XANES results in that day 7 biotic oxidation product shows less Fe(II) than the abiotic product though the difference may not be significant due to noise in spectra (69.1 ± 3.9 vs 74.0 ± 1.1%) (Figure 5A and Table S2). These results from scaled-up cultures (250 mL) may not fully agree with the phenanthroline data from small batch (80 mL) cultures because the different headspace volume and vessel geometry could affect oxygen diffusion, which could result in different oxidation rates. Altogether, our results suggest that microbes can catalyze faster smectite oxidation than abiotic exposure to oxygen, but further characterization is needed to understand the conditions under which this occurs.

Local Structural Changes from Biotic and Abiotic Oxidation. The oxidation of Fe(II) causes a charge imbalance in the octahedral sheet of smectite, which could cause some Fe(III) to be ejected from the structure and precipitate as Fe(III) (oxyhydr)oxide.[59] To test if there is secondary Fe(III) (oxyhydr)oxide formation, we analyzed the same samples using MBS at lower temperatures, including 13 and 5 K (Figures 5B and S7), at which secondary Fe(III) (oxyhydr)oxides would be expected to form a sextet. The unaltered clay shows a doublet at 13 K, which corresponds to the dominantly ferrous components. The day 7 13 K spectra fit shows a small proportion of a partially collapsed Fe(III) "sextet" (labeled as

https://doi.org/10.1021/acs.est.2c05142
Environ. Sci. Technol. XXXX, XXX, XXX−XXX

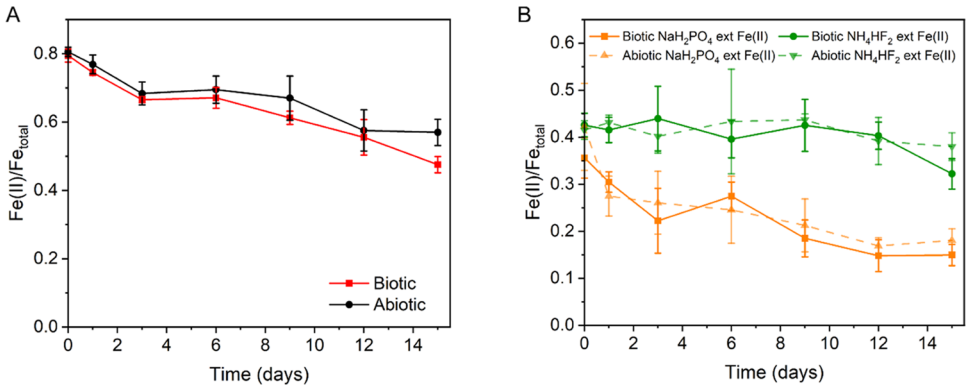

Figure 3. (A) Fe(II)/Fe_{total} change during biotic and abiotic smectite oxidation; (B) the change of reactive edge-Fe(II) + partial interior-Fe(II) (extracted by NaH_2PO_4) and less-reactive interior-Fe(II) (extracted by NH_4HF_2) by biotic and abiotic smectite oxidation (solid line: biotic, dashed line: abiotic). The data were obtained from the phenanthroline assay.

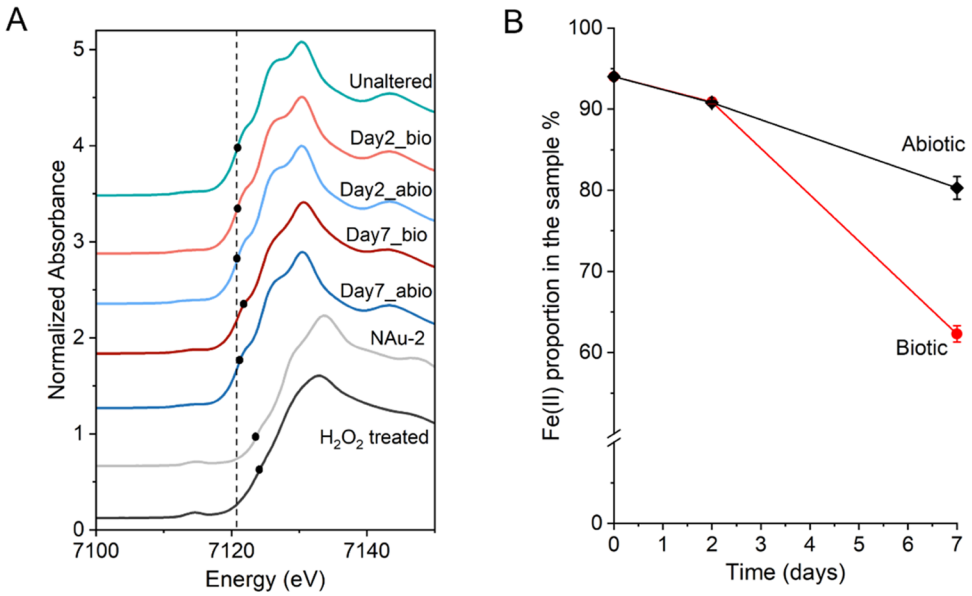

Figure 4. (A) Fe K-edge XANES of Fe(II)-smectite after biotic and abiotic oxidation at different time points. Black dots indicate the Fe K-edge positions, defined as the energy at which normalized absorbance is 0.5. The dashed line indicates the Fe K-edge position of unaltered smectite. (B) Proportion of Fe(II) left in biotic and abiotic oxidation products collected at different time points (unaltered, day 2 and day 7) obtained from linear combination fitting (LCF). H_2O_2-treated smectite XANES data were obtained using the same mineral under the same media condition.

(b)Ferric; 16% in day7_bio and 10.9% in day7_abio). To thoroughly evaluate the possibility of ferrihydrite (Fh), we tried to force a larger ferrihydrite component during fitting and could accommodate at most 6.6% (day7_bio) and 1.8% (day7_abio) without decreasing the goodness of the fit (Chi∧2). However, the fitting program optimally includes less than 0.03% Fh in both sample fits, suggesting that any secondary Fe(III) oxyhydroxide formation is likely minor and could be explained by oxidation of minor dissolved Fe(II) in solution and that the vast majority of the Fe(III) formed was retained in the smectite structure (detailed fitting description is provided in the SI section 2.3.3).

To further investigate the fate of oxidized iron, the unaltered smectite and its oxidation products were studied using EXAFS spectroscopy. Iron oxidation should produce local structural changes, specifically contractions in interatomic distances caused by the smaller ionic radius of Fe(III) compared to Fe(II). In addition, a mixture of octahedral iron in both ferrous and ferric oxidation states should increase the apparent disorder of neighboring shells of atoms as determined by EXAFS spectroscopy. For the unaltered smectite, the average distance between iron and oxygen that comprises its first coordination shell was 2.10 Å (Table S4), which is consistent with other reports.[51,59] The Fe−O distance contracted to 2.07 Å in the biotic oxidation product on day 7, which is the most oxidized sample. This sample also showed an increase in disorder in the oxygen shell (σ^2 = 0.015 for Fe−O), as would be expected for coexisting Fe(II) and Fe(III). The interatomic distance between Fe and the octahedral sheet cations (Fe, Mg, and Al) does not display a significant contraction (Table S4). The coordination number (N) for the unaltered sample is consistent with Fe fully contained in the octahedral sheet and was modeled as a random distribution of the neighboring cations as determined from the smectite chemical formula. For the oxidized samples, all spectra were well fitted by holding these *N* values constant (Figure 6). The Debye−Waller factor (σ^2, a measure of disorder) increased slightly for the most oxidized samples (Table S4). The interatomic distances contracted and Debye−Waller factors slightly increased for the Fe−Si shells for the most oxidized samples. These

https://doi.org/10.1021/acs.est.2c05142
Environ. Sci. Technol. XXXX, XXX, XXX−XXX

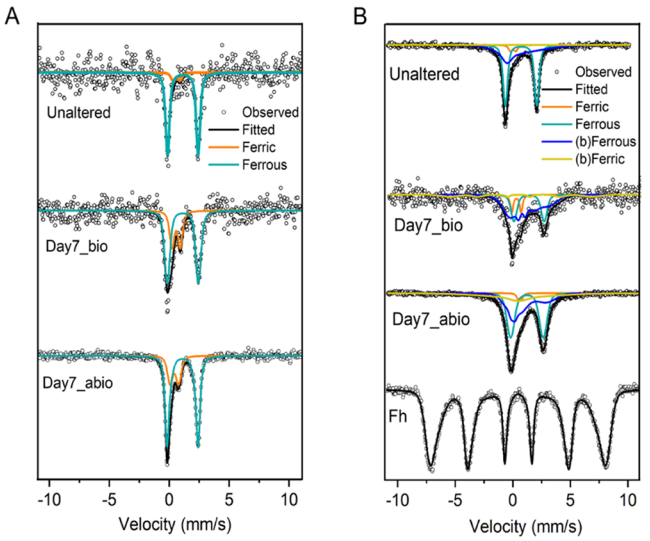

Figure 5. Mössbauer spectra with fitting at (A) 295 K and (B) 13 K of the unaltered, biotic, and abiotic oxidation samples harvested on day 7. The ferrihydrite (Fh) spectrum was obtained from Noor and Thompson[70] and is shown as a reference for sextet at 13 K. Full datasets of MBS at 295, 13, and 5 K are given in the SI (Figures S5–S7, Tables S2 and S3).

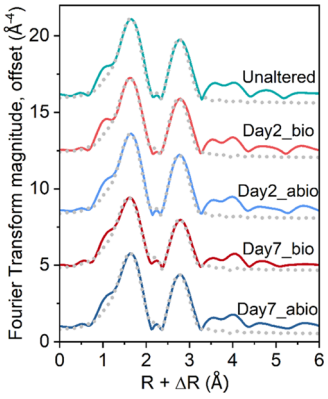

Figure 6. Fourier transforms of EXAFS spectra. Modeled fits (shown as gray dots) were calculated using the *R* range from 1–3.3 Å. The k^3-weighted EXAFS spectra before Fourier transforms are shown in Figure S8.

observations are fully consistent with Fe(III) being retained in the octahedral sheet of the smectite. These measurements indicate that moderate smectite Fe(II) oxidation can be accommodated by local structural changes while supporting microbial growth.

Expression of Fe(II) Oxidation Genes by ES-1 in Smectite Culture vs Fe(II)-Citrate Culture. ES-1 has two types of Fe(II) oxidases, Cyc2 (in three versions: Cyc2_1, Cyc2_2, and Cyc2_3) and MtoA. To clarify the roles of these Fe(II) oxidases in solid and aqueous Fe(II) oxidation, RT-qPCR was applied to quantify the gene expression level of the three *cyc2* genes and *mtoA* in Fe(II)-citrate and smectite cultures (Figure 7 and Table S5). Samples were taken from mid-log and late-log growth phases in Fe(II)-citrate and smectite cultures; then, the Fe(II) source was switched and one more set of samples was taken after the switch. The RT-qPCR data show that *cyc2_1* and *mtoA* were upregulated ($p < 0.05$, *t*-test), while *cyc2_2* and *cyc2_3* were downregulated in smectite culture vs Fe(II)-citrate culture in the single Fe source experiment ($p < 0.05$, *t*-test). In particular, *mtoA* expression in mid-log smectite culture was 23× higher than that in Fe(II)-citrate culture ($p < 0.05$, *t*-test) (Table S5). Further the Fe source switching experiment also showed upregulation of *cyc2_1* and *mtoA* when switched from Fe(II)-citrate culture to smectite culture and upregulation of *cyc2_2* and *cyc2_3* when switched from smectite culture to Fe(II)-citrate culture. The RT-qPCR data imply that Cyc2 and MtoA play different roles in oxidizing aqueous and solid Fe(II).

Expression of Cyc2 and Mto Pathways in Fe(II)-Smectite Culture vs Fe(II)-Citrate Culture. To test the expression of iron oxidases, proteomics was performed on ES-1 grown on Fe(II)-smectite and Fe(II)-citrate. All Cyc2 proteins (Cyc2_1, Cyc2_2, and Cyc2_3) were detected in both Fe(II)-citrate and smectite samples, and the differential protein expression analysis shows that Cyc2_1 and Cyc2_3 are less abundant when ES-1 is grown on smectite than on Fe(II)-citrate (two-sample *t*-test, $p \leq 0.05$) (Table 1). None of the proteins involved in the Mto pathway were detected in the Fe(II)-citrate samples, while in the smectite cultures, we identified MtoB and the monoheme cytochrome c (Uniprot entry: D5CMP7) encoded by the gene Slit_2494 in the *mto* operon (Table 1). Since the porin is unstable by itself and cannot exist without the cytochrome,[71] it is reasonable to propose that MtoA is expressed together with MtoB in the smectite culture. The lack of MtoA detection is likely due to the strong disulfide bonds between cysteines and 10 heme groups, so the protein cannot be efficiently denatured and accurately identified by mass spectrometry. The proteomes of the Fe(II)-citrate culture have much higher number of detected proteins compared to smectite yet show no Mto-related proteins (Table S6). Thus, we conclude that the Mto pathway is expressed for smectite oxidation but not for Fe(II)-citrate oxidation. The RT-qPCR and proteomics patterns correspond well and together provide evidence that the Mto pathway is involved in solid Fe(II) oxidation, while Cyc2 mainly contributes to aqueous Fe(II) oxidation.

DISCUSSION

The constant process of Earth's crustal weathering produces trioctahedral Fe(II)-smectite,[9,10] which could represent a widely available substrate for microbial growth. Yet, its potential as an electron donor for microbial Fe oxidation has not previously been explored because trioctahedral Fe(II)-smectites are not generally available for experimentation. As a result, most knowledge about microbial Fe(II) clay oxidation comes from artificially reduced dioctahedral Fe(III)-smectites,[20−22] which has yielded initial promising evidence that microbes can oxidize clays. However, these clays may not behave similarly because Fe distribution in the structure is significantly different. Unlike dioctahedral clays, the octahedral sheet of a trioctahedral smectite is fully occupied, allowing for more adjacent Fe atoms, which could lead to faster electron-transfer rates and better performance as an electron donor. Here, we synthesized a trioctahedral Fe(II)-smectite and demonstrated substantial growth of the FeOB *S. lithotrophicus* ES-1 using clay-bound Fe(II). Our results showed that *S. lithotrophicus* ES-1 uses the solid Fe(II) in smectite to produce biomass (Figures 1 and 2) and may accelerate mineral Fe(II) oxidation under certain conditions (Figure 4).

To grow on smectite, FeOB need mechanisms to interact with minerals. Previous studies on FeRB proposed that bacterial cells can access solid Fe(III)-minerals, including

https://doi.org/10.1021/acs.est.2c05142
Environ. Sci. Technol. XXXX, XXX, XXX−XXX

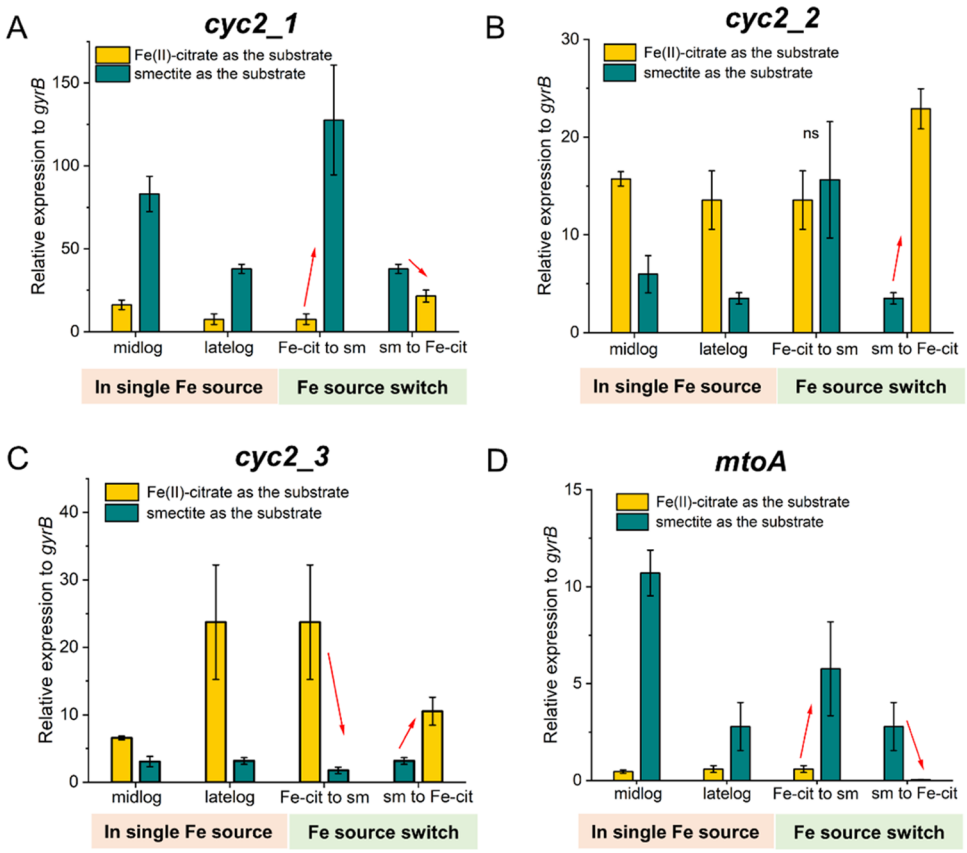

Figure 7. Relative expression by RT-qPCR of (A) *cyc2_1*, (B) *cyc2_2*, (C) *cyc2_3*, and (D) *mtoA* to reference *gyrB* when ES-1 was grown on Fe(II)-citrate and smectite; ns: not significant ($p > 0.05$, *t*-test). If not specified as "ns". the difference between the two groups is significant ($p \leq 0.05$, *t*-test). The error bars represent standard deviation of biological triplicates.

Table 1. Differential Expression Analysis (Smectite vs Fe(II)-Citrate) of Proteins Involved in Fe(II) Oxidation[a,b,c]

			maximum percentile			
protein name	locus tag	function	smectite	Fe(II)-citrate	log 2fold change (smectite vs Fe(II) citrate)	*p*-value
Cyc2_1	Slit_0263	Fe(II) oxidation	96.3	99.7	−2.73	0.003
Cyc2_2	Slit_0264	Fe(II) oxidation	97.5	98.9	ns	ns
Cyc2_3	Slit_0265	Fe(II) oxidation	69.2	92.1	−4.01	0.00
MtoB	Slit_2496	Porin of MtoAB Fe(II) oxidase	64.8	0	4.07	0.03
D5CMP7	Slit_2494	monoheme cytochrome c	33.5	0	2.16	0.04

[a]D5CMP7: encoded by a gene downstream of CymA. [b]Maximum percentile was calculated from ranking the iBAQ values. [c]ns: not significant from the two-sample *t*-test, $p > 0.05$.

smectite, by direct contact and/or electron shuttles.[72−76] Unlike the FeRB *Shewanella oneidensis*, ES-1 does not have a known organic electron shuttle (riboflavin) transporting system. However, ES-1 does possess the Mto pathway, which includes an outer-membrane multiheme cytochrome[27,77,78] that could enable direct contact to oxidize smectite-bound Fe(II). MtoAB is a decaheme cytochrome-porin complex homologous to the Fe(III)-reducing MtrAB in *S. oneidensis*, in which multiple hemes conduct electrons across the outer membrane,[29,77] thus enabling interactions with extracellular electron sources/sinks. ES-1 expressed Mto pathway proteins on smectite but not on Fe(II)-citrate, which supports a model in which ES-1 directly accesses the solid Fe(II) in smectite using MtoAB (Figure 8A).

In addition to MtoAB, the smectite-grown cells also express Cyc2 (Table 1), including substantial expression of all three Cyc2 proteins, suggesting that they also play a role in smectite oxidation. Cyc2 has a single heme, implying it is an oxidase of dissolved Fe(II).[77] Dissolved Fe(II) could shuttle electrons from smectite to cells. Previous findings in abiotic systems have demonstrated the interfacial electron transfer between Fe(III) and structural Fe in clays.[79,80] Fe(III) produced from dissolved Fe(II) oxidation could therefore be re-reduced to Fe(II) through interfacial electron transfer, as suggested by a previous study on microbial biotite oxidation.[26] Herein, we propose two possible mechanisms for ES-1 smectite oxidation: (1) direct contact to acquire electrons from mineral-bound Fe(II) via multiheme−porin complex MtoAB and (2) indirect oxidation with the involvement of dissolved Fe(II) by Cyc2 (Figure 8A).

Microbial growth is likely a function of smectite mineralogy. Fe(II) is in the middle octahedral layer, sandwiched by two silicate tetrahedral sheets. Previous studies have demonstrated that Fe in edge sites is the most reactive and is accessible to microbes.[37,67,72] However, it is not well-known whether

https://doi.org/10.1021/acs.est.2c05142
Environ. Sci. Technol. XXXX, XXX, XXX−XXX

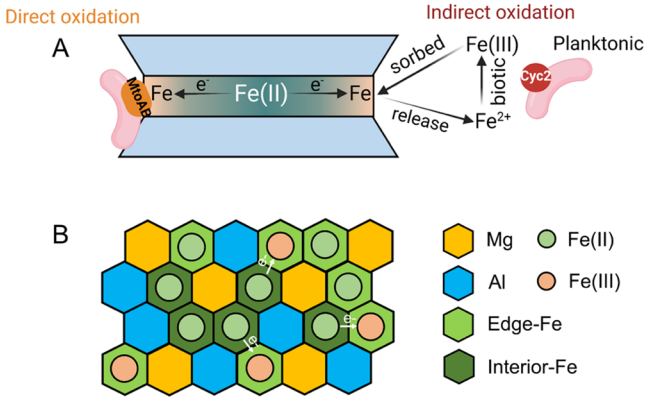

Figure 8. (A) Proposed molecular mechanism of ES-1 grown on Fe(II)-smectite; (B) plan view of the middle trioctahedral layer in the smectite structure. The cations represent the actual metal composition of the synthetic smectite.

microbes can oxidize interior-Fe(II) though this would clearly affect the extent to which microbes can oxidize smectite. Our results show that ES-1 can use some interior-Fe(II) (Figure 2). This suggests electron transfer between the interior- and edge-Fe (Figure 8B), which has been intensively characterized in abiotic systems.[35,38−43] Although microbes can use the interior-Fe, we observed only partial oxidation and a two-stage process (fast to slow reaction) during incubation, which are consistent with previous observations in abiotic systems.[34,35,37,43,59,81] The rapid decrease of NaH_2PO_4-extractable Fe(II) during days 0−3 is primarily due to the consumption of reactive edge-Fe(II) by ES-1 (Figure 2). Then, the oxidation rate could be constrained by the electron hopping rate from less-reactive interior-Fe to the edge sites (Figure 8B). Since the driving force of electron hopping is the redox potential gradient between the interior- and edge-Fe,[35,82,83] with the oxidation process, the redox potential gradient could decrease until reaching an equilibrium, which causes the decrease of reaction rate and incomplete oxidation. Partial oxidation results in mixed valent trioctahedral smectite (Figure 8B), with only minor structural changes and no detectable secondary mineral formation (Figures 5B and 6). This mixed valent smectite may then be available for microbial Fe reduction. In this way, trioctahedral Fe(II)-smectite can act as a geobattery to connect the redox cycles between FeOB and FeRB.

Environmental Implications. Iron-bearing smectites are practically ubiquitous in soils and sediments, where they can support microbial life and catalyze environmentally significant processes. Previous studies have established that FeRB can reduce Fe(III) in smectite,[32,33,84−86] and resulting redox changes alter the reactivity of smectites toward metals and organic contaminants.[7,32,33,37,87] Our work showed that trioctahedral Fe(II)-smectite can be used as an electron source to support the growth of a common, widely distributed microaerophilic Fe(II) oxidizer. Biotic Fe(II) oxidation may result in accelerated smectite Fe(II) oxidation under some conditions but not others, and yet, in either case, smectite oxidation fuels growth. This suggests that mineral Fe(II) measurements cannot always distinguish biotic versus abiotic effects, potentially rendering biotic effects invisible, thus emphasizing the need for gene-based markers of microbe−mineral interactions. As smectite Fe(II) oxidation can support the growth of FeOB, this is another way in which clays can fuel nutrient cycling in subsurface settings. FeOB and FeRB can coexist in sediment redox transition zones,[88,89] with autotrophic FeOB using energy from smectite Fe(II) oxidation to fix carbon and FeRB respiring these organics, coupled to smectite Fe(III) reduction. In this way, smectites can support both FeOB and FeRB growth and drive C and N biogeochemical cycling. In turn, FeOB and FeRB can modulate redox and charge of smectites and their reactivity, including sorption and degradation of contaminants.

Intriguingly, FeOB and FeRB appear to use similar mechanisms to oxidize and reduce smectite clays. Our work and previous studies have demonstrated that the multiheme cytochrome−porin Mto/MtrAB homologues mediate electron transfer between microbes and Fe minerals. Mto/MtrAB homologues are widely distributed among bacteria,[90] so Mto/Mtr-based extracellular electron transfer may be a common mechanism that bacteria evolved to access solid electron sources/sinks. *S. lithotrophicus* ES-1 has not only Cyc2 and MtoAB but also other multiheme cytochrome genes that may also be useful in accessing additional solid substrates. Such a diverse toolkit may allow FeOB like ES-1 to adapt to changing Fe dynamics, thus playing an important role in sustaining life on geomaterials across diverse habitats.

■ ASSOCIATED CONTENT

Supporting Information

The Supporting Information is available free of charge at https://pubs.acs.org/doi/10.1021/acs.est.2c05142.

Additional TEM images; data on dissolved Fe(II) release; MBS data collected at lower temperatures; method details on culturing, MBS fitting, and proteomics (PDF)

■ AUTHOR INFORMATION

Corresponding Author

Clara S. Chan − *School of Marine Science and Policy and Department of Earth Sciences, University of Delaware, Newark, Delaware 19716, United States;* orcid.org/0000-0003-1810-4994; Email: cschan@udel.edu

Authors

Nanqing Zhou − *School of Marine Science and Policy, University of Delaware, Newark, Delaware 19716, United States*

Robert J. Kupper − *Department of Earth and Planetary Sciences, Washington University in St. Louis, Saint Louis, Missouri 63130, United States*

Jeffrey G. Catalano − *Department of Earth and Planetary Sciences, Washington University in St. Louis, Saint Louis, Missouri 63130, United States;* orcid.org/0000-0001-9311-977X

Aaron Thompson − *Department of Crop and Soil Sciences, University of Georgia, Athens, Georgia 30602, United States;* orcid.org/0000-0001-6301-7377

Complete contact information is available at: https://pubs.acs.org/10.1021/acs.est.2c05142

Notes

The authors declare no competing financial interest.

https://doi.org/10.1021/acs.est.2c05142
Environ. Sci. Technol. XXXX, XXX, XXX−XXX

■ ACKNOWLEDGMENTS

This work was funded by NASA Exobiology Grant 80NSSC18K1292 and NSF BIO Grant 1817651 to CSC and the UD Dissertation Fellowship to N.Z. We thank Shannon Modla from the UD BioImaging Center for TEM imaging. We thank Yanbao Yu and the Mass Spectrometry Facility in the University of Delaware for the proteomic analysis, which is supported by National Institute of General Medical Sciences or the National Institutes of Health under Award Number P20GM104316. Comments from three anonymous reviewers improved this manuscript.

■ REFERENCES

(1) Odom, I. E. Smectite Clay Minerals: Properties and Uses. *Philos. Trans. R. Soc., A* **1984**, *311*, 391−409.
(2) Chen, N.; Fang, G.; Zhu, C.; Wu, S.; Liu, G.; Dionysiou, D. D.; Wang, X.; Gao, J.; Zhou, D. Surface-Bound Radical Control Rapid Organic Contaminant Degradation through Peroxymonosulfate Activation by Reduced Fe-Bearing Smectite Clays. *J. Hazard. Mater.* **2020**, *389*, No. 121819.
(3) Chen, N.; Fang, G.; Liu, G.; Zhou, D.; Gao, J.; Gu, C. The Degradation of Diethyl Phthalate by Reduced Smectite Clays and Dissolved Oxygen. *Chem. Eng. J.* **2019**, *355*, 247−254.
(4) Zeng, Q.; Dong, H.; Wang, X.; Yu, T.; Cui, W. Degradation of 1, 4-Dioxane by Hydroxyl Radicals Produced from Clay Minerals. *J. Hazard. Mater.* **2017**, *331*, 88−98.
(5) Qafoku, O.; Pearce, C. I.; Neumann, A.; Kovarik, L.; Zhu, M.; Ilton, E. S.; Bowden, M. E.; Resch, C. T.; Arey, B. W.; Arenholz, E.; Felmy, A. R.; Rosso, K. M. Tc(VII) and Cr(VI) Interaction with Naturally Reduced Ferruginous Smectite from a Redox Transition Zone. *Environ. Sci. Technol.* **2017**, *51*, 9042−9052.
(6) Latta, D. E.; Boyanov, M. I.; Kemner, K. M.; O'Loughlin, E. J.; Scherer, M. M. Abiotic Reduction of Uranium by Fe(II) in Soil. *Appl. Geochem.* **2012**, *27*, 1512−1524.
(7) O'loughlin, E. J.; Boyanov, M. I.; Kemner, K. M.; Thalhammer, K. O. Reduction of Hg(II) by Fe(II)-Bearing Smectite Clay Minerals. *Minerals* **2020**, *10*, 1079.
(8) Anderson, D. W. The Effect of Parent Material and Soil Development on Nutrient Cycling in Temperate Ecosystems. *Biogeochemistry* **1988**, *5*, 71−97.
(9) Andrews, A. J. Saponite and Celadonite in Layer 2 Basalts, DSDP Leg 37. *Contrib Mineral Petrol.* **1980**, *73*, 323−340.
(10) Kristmannsdottir, H. Alteration of Basaltic Rocks by Hydrothermal-Activity at 100-300 °C. *Dev. Sedimentol.* **1979**, *27*, 359−367.
(11) Teagle, D. A. H.; Alt, J. C.; Bach, W.; Halliday, A. N.; Erzinger, J.Alteration of Upper Ocean Crust in a Ridge-Flank Hydrothermal Upflow Zone: Mineral, Chemical, and Isotopic Constraints from Hole 896A. In *Proceedings of the Ocean Drilling Program, Scientific Results*; Ocean Drilling Program, 1996; Vol. *148* DOI: 10.2973/odp.proc.sr.148.113.1996.
(12) Alt, J. C.; Honnorez, J.; Laverne, C.; Emmermann, R. Hydrothermal Alteration of a 1 Km Section through the Upper Oceanic Crust, Deep Sea Drilling Project Hole 504B: Mineralogy, Chemistry and Evolution of Seawater-Basalt Interactions. *J. Geophys. Res.* **1986**, *91*, 10309.
(13) Alt, J. C.; Teagle, D. A. H. Hydrothermal Alteration of Upper Oceanic Crust Formed at a Fast-Spreading Ridge: Mineral, Chemical, and Isotopic Evidence from ODP Site 801. *Chem. Geol.* **2003**, *201*, 191−211.
(14) April, R. H.; Keller, D. M. Saponite and Vermiculite in Amygdales of the Granby Basaltic Tuff, Connecticut Valley. *Clays Clay Miner.* **1992**, *40*, 22−31.
(15) Badaut, D.; Decarreau, A.; et al. Occurrence of a Ferrous, Trioctahedral Smectite in Recent Sediments of Atlantis II Deep, Red Sea. *Clay Miner.* **1985**, *20*, 389−404.
(16) Parthasarathy, G.; Choudary, B. M.; Sreedhar, B.; Kunwar, A. C.; Srinivasan, R. Ferrous Saponite from the Deccan Trap, India, and Its Application in Adsorption and Reduction of Hexavalent Chromium. *Am. Mineral.* **2003**, *88*, 1983−1988.
(17) Emerson, D.; Merrill Floyd, M.Enrichment and Isolation of Iron-Oxidizing Bacteria at Neutral PH. In *Methods Enzymology* 2005; Vol. *397*, pp 112−123 DOI: 10.1016/S0076-6879(05)97006-7.
(18) Emerson, D.; Rentz, J. A.; Lilburn, T. G.; Davis, R. E.; Aldrich, H.; Chan, C.; Moyer, C. L. A Novel Lineage of Proteobacteria Involved in Formation of Marine Fe-Oxidizing Microbial Mat Communities. *PLoS One* **2007**, *2*, No. e667.
(19) Jiao, Y.; Kappler, A.; Croal, L. R.; Newman, D. K. Isolation and Characterization of a Genetically Tractable Photoautotrophic Fe(II)-Oxidizing Bacterium, Rhodopseudomonas Palustris Strain TIE-1. *Appl Environ Microbiol* **2005**, *71*, 4487−4496.
(20) Zhao, L.; Dong, H.; Kukkadapu, R.; Agrawal, A.; Liu, D.; Zhang, J.; Edelmann, R. E. Biological Oxidation of Fe(II) in Reduced Nontronite Coupled with Nitrate Reduction by Pseudogulbenkiania Sp. Strain 2002. *Geochim. Cosmochim. Acta* **2013**, *119*, 231−247.
(21) Zhang, L.; Dong, H.; Kukkadapu, R. K.; Jin, Q.; Kovarik, L. Electron Transfer between Sorbed Fe(II) and Structural Fe(III) in Smectites and Its Effect on Nitrate-Dependent Iron Oxidation by Pseudogulbenkiania Sp. Strain 2002. *Geochim. Cosmochim. Acta* **2019**, *265*, 132−147.
(22) Zhao, L.; Dong, H.; Kukkadapu, R. K.; Zeng, Q.; Edelmann, R. E.; Pentrák, M.; Agrawal, A. Biological Redox Cycling of Iron in Nontronite and Its Potential Application in Nitrate Removal. *Environ. Sci. Technol.* **2015**, *49*, 5493−5501.
(23) Carlson, H. K.; Clark, I. C.; Blazewicz, S. J.; Iavarone, A. T.; Coates, J. D. Fe(II) Oxidation Is an Innate Capability of Nitrate-Reducing Bacteria That Involves Abiotic and Biotic Reactions. *J. Bacteriol.* **2013**, *195*, 3260−3268.
(24) Klueglein, N.; Zeitvogel, F.; Stierhof, Y. D.; Floetenmeyer, M.; Konhauser, K. O.; Kappler, A.; Obst, M. Potential Role of Nitrite for Abiotic Fe(II) Oxidation and Cell Encrustation during Nitrate Reduction by Denitrifying Bacteria. *Appl. Environ. Microbiol.* **2014**, *80*, 1051−1061.
(25) Grabb, K. C.; Buchwald, C.; Hansel, C. M.; Wankel, S. D. A Dual Nitrite Isotopic Investigation of Chemodenitrification by Mineral-Associated Fe (II) and Its Production of Nitrous Oxide. *Geochim. Cosmochim. Acta* **2017**, *196*, 388−402.
(26) Shelobolina, E.; Xu, H.; Konishi, H.; Kukkadapu, R.; Wu, T.; Blöthe, M.; Roden, E. Microbial Lithotrophic Oxidation of Structural Fe(II) in Biotite. *Appl. Environ. Microbiol.* **2012**, *78*, 5746−5752.
(27) Emerson, D.; Field, E. K.; Chertkov, O.; Davenport, K. W.; Goodwin, L.; Munk, C.; Nolan, M.; Woyke, T. Comparative Genomics of Freshwater Fe-Oxidizing Bacteria: Implications for Physiology, Ecology, and Systematics. *Front. Microbiol.* **2013**, *4*, 1−17.
(28) He, S.; Barco, R. A.; Emerson, D.; Roden, E. E. Comparative Genomic Analysis of Neutrophilic Iron(II) Oxidizer Genomes for Candidate Genes in Extracellular Electron Transfer. *Front. Microbiol.* **2017**, *8*, No. 1584.
(29) Liu, J.; Wang, Z.; Belchik, S. M.; Edwards, M. J.; Liu, C.; Kennedy, D. W.; Merkley, E. D.; Lipton, M. S.; Butt, J. N.; Richardson, D. J.; Zachara, J. M.; Fredrickson, J. K.; Rosso, K. M.; Shi, L. Identification and Characterization of MtoA: A Decaheme c-Type Cytochrome of the Neutrophilic Fe(Ll)-Oxidizing Bacterium *Sideroxydans Lithotrophicus* ES-1. *Front. Microbiol.* **2012**, *3*, No. 37.
(30) McAllister, S. M.; Polson, S. W.; Butterfield, D. A.; Glazer, B. T.; Sylvan, J. B.; Chan, C. S. Validating the Cyc2 Neutrophilic Iron Oxidation Pathway Using Meta-Omics of Zetaproteobacteria Iron Mats at Marine Hydrothermal Vents. *mSystems* **2020**, *5*, No. e00553-19.
(31) Zhou, N.; Keffer, J. L.; Polson, S. W.; Chan, C. S. Unraveling Fe(II)-Oxidizing Mechanisms in a Facultative Fe(II) Oxidizer, *Sideroxydans Lithotrophicus* Strain ES-1, via Culturing, Transcriptomics, and Reverse Transcription-Quantitative PCR. *Appl. Environ. Microbiol.* **2022**, *88*, No. e01595-21.
(32) Jaisi, D. P.; Kukkadapu, R. K.; Eberl, D. D.; Dong, H. Control of Fe(III) Site Occupancy on the Rate and Extent of Microbial

https://doi.org/10.1021/acs.est.2c05142
Environ. Sci. Technol. XXXX, XXX, XXX−XXX

Reduction of Fe(III) in Nontronite. *Geochim. Cosmochim. Acta* **2005**, *69*, 5429−5440.
(33) Zhang, G.; Senko, J. M.; Kelly, S. D.; Tan, H.; Kemner, K. M.; Burgos, W. D. Microbial Reduction of Iron(III)-Rich Nontronite and Uranium(VI). *Geochim. Cosmochim. Acta* **2009**, *73*, 3523−3538.
(34) Neumann, A.; Petit, S.; Hofstetter, T. B. Evaluation of Redox-Active Iron Sites in Smectites Using Middle and near Infrared Spectroscopy. *Geochim. Cosmochim. Acta* **2011**, *75*, 2336−2355.
(35) Liao, W.; Yuan, S.; Liu, X.; Tong, M. Anoxic Storage Regenerates Reactive Fe(II) in Reduced Nontronite with Short-Term Oxidation. *Geochim. Cosmochim. Acta* **2019**, *257*, 96−109.
(36) Noda, N.; Yamashita, S.; Takahashi, Y.; Matsumoto, M.; Enokido, Y.; Amano, K.; Kawai, T.; Sakuma, H.; Fukushi, K.; Sekine, Y.; Nakamura, T. Anaerobic Microscopic Analysis of Ferrous Saponite and Its Sensitivity to Oxidation by Earth's Air: Lessons Learned for Analysis of Returned Samples from Mars and Carbonaceous Asteroids. *Minerals* **2021**, *11*, 1244.
(37) Neumann, A.; Hofstetter, T. B.; Lüssi, M.; Cirpka, O. A.; Petit, S.; Schwarzenbach, R. P. Assessing the Redox Reactivity of Structural Iron in Smectites Using Nitroaromatic Compounds As Kinetic Probes. *Environ. Sci. Technol.* **2008**, *42*, 8381−8387.
(38) Schaefer, M. V.; Gorski, C. A.; Scherer, M. M. Spectroscopic Evidence for Interfacial Fe(II)-Fe(III) Electron Transfer in a Clay Mineral. *Environ. Sci. Technol.* **2011**, *45*, 540−545.
(39) Latta, D. E.; Neumann, A.; Premaratne, W. A. P. J.; Scherer, M. M. Fe(II)−Fe(III) Electron Transfer in a Clay Mineral with Low Fe Content. *ACS Earth Space Chem.* **2017**, *1*, 197−208.
(40) Neumann, A.; Olson, T. L.; Scherer, M. M. Spectroscopic Evidence for Fe(II)-Fe(III) Electron Transfer at Clay Mineral Edge and Basal Sites. *Environ. Sci. Technol.* **2013**, *47*, 6969−6977.
(41) Alexandrov, V.; Neumann, A.; Scherer, M. M.; Rosso, K. M. Electron Exchange and Conduction in Nontronite from First-Principles. *J. Phys. Chem. C* **2013**, *117*, 2032−2040.
(42) Shi, B.; Liu, K.; Wu, L.; Li, W.; Smeaton, C. M.; Beard, B. L.; Johnson, C. M.; Roden, E. E.; Van Cappellen, P. Iron Isotope Fractionations Reveal a Finite Bioavailable Fe Pool for Structural Fe(III) Reduction in Nontronite. *Environ. Sci. Technol.* **2016**, *50*, 8661−8669.
(43) Yuan, S.; Liu, X.; Liao, W.; Zhang, P.; Wang, X.; Tong, M. Mechanisms of Electron Transfer from Structrual Fe(II) in Reduced Nontronite to Oxygen for Production of Hydroxyl Radicals. *Geochim. Cosmochim. Acta* **2018**, *223*, 422−436.
(44) Jewell, T. N. M.; Karaoz, U.; Brodie, E. L.; Williams, K. H.; Beller, H. R. Metatranscriptomic Evidence of Pervasive and Diverse Chemolithoautotrophy Relevant to C, S, N and Fe Cycling in a Shallow Alluvial Aquifer. *ISME J.* **2016**, *10*, 2106−2117.
(45) Nakagawa, K.; Murase, J.; Asakawa, S.; Watanabe, T. Involvement of Microaerophilic Iron-Oxidizing Bacteria in the Iron-Oxidizing Process at the Surface Layer of Flooded Paddy Field Soil. *J. Soils Sediments* **2020**, *20*, 4034−4041.
(46) Herrmann, M.; Opitz, S.; Harzer, R.; Totsche, K.; Küsel, K. Attached and Suspended Denitrifier Communities in Pristine Limestone Aquifers Harbor High Fractions of Potential Autotrophs Oxidizing Reduced Iron and Sulfur Compounds. *Microbial. Ecol.* **2017**, *74*, 264−277.
(47) Krauze, P.; Kämpf, H.; Horn, F.; Liu, Q.; Voropaev, A.; Wagner, D.; Alawi, M. Microbiological and Geochemical Survey of Co2-Dominated Mofette and Mineral Waters of the Cheb Basin, Czech Republic. *Front. Microbiol.* **2017**, *8*, No. 2446.
(48) Roden, E. E.; McBeth, J. M.; Blöthe, M.; Percak-Dennett, E. M.; Fleming, E. J.; Holyoke, R. R.; Luther, G. W.; Emerson, D.; Schieber, J. The Microbial Ferrous Wheel in a Neutral PH Groundwater Seep. *Front. Microbiol.* **2012**, *3*, 1−18.
(49) Naruse, T.; Ban, Y.; Yoshida, T.; Kato, T.; Namikawa, M.; Takahashi, T.; Nishida, M.; Asakawa, S.; Watanabe, T. Community Structure of Microaerophilic Iron-Oxidizing Bacteria in Japanese Paddy Field Soils. *Soil Sci. Plant Nutr.* **2019**, *65*, 460−470.
(50) Decarreau, A.; Bonnin, D.; Badaut-Trauth, D.; Couty, R.; Kaiser, P. Synthesis and Crystallogenesis of Ferric Smectite by Evolution of Si-Fe Coprecipitates in Oxidizing Conditions. *Clay Miner.* **1987**, *22*, 207−223.
(51) Chemtob, S. M.; Nickerson, R. D.; Morris, R. V.; Agresti, D. G.; Catalano, J. G. Synthesis and Structural Characterization of Ferrous Trioctahedral Smectites: Implications for Clay Mineral Genesis and Detectability on Mars. *J. Geophys. Res. E: Planets* **2015**, *120*, 1119−1140.
(52) Kodama, H.; De Kimpe, C. R.; Dejou, J. Ferrian Saponite in a Gabbro Saprolite at Mont MéGantic, Quebec. *Clays Clay Miner.* **1988**, *36*, 102−110.
(53) Kimbara, K.; Honda, S. An Iron-Rich Saponite-like Mineral Found in the Moriyama Volcanic Rocks, Gojome, Akita Prefecture, Japan. *Bull. Geol. Surv. Japan* **1975**, *36*, 102−110.
(54) Daynyak, L. G.; Drits, V. A.; Kudryavtsev, D. I.; Simanovich, I. M.; Slonimskaya, M. V. Crystal Chemical Specificity of Trioctahedral Smectites: Products of Secondary Alteration of Oceanic and Continental Basalts. *Dokl. Akad. Nauk SSSR* **1981**, *259*, 1458−1462.
(55) Despraires, A.; Tremblay, P.; Laloy, C. Secondary Mineral Assemblages in a Volcanic Sequence Drilled during Odp Leg 104 in the Norwegian Sea. *Proc. Ocean Drill. Program: Sci. Results* **1989**, *104*, 397−409.
(56) Stucki, J. W. The Quantitative Assay of Minerals for Fe 2+ and Fe 3+ Using 1,10-Phenanthroline: II. A Photochemical Method. *Soil Sci. Soc. Am. J.* **1981**, *45*, 638−641.
(57) Rancourt, D. G.; Ping, J. Y. Voigt-Based Methods for Arbitrary-Shape Static Hyperfine Parameter Distributions in Mössbauer Spectroscopy. *Nucl. Instrum. Methods Phys. Res., Sect. B* **1991**, *58*, 85−97.
(58) Ravel, B.; Newville, M. ATHENA and ARTEMIS Interactive Graphical Data Analysisusing IFEFFIT. *Phys. Scr.* **2005**, *T115*, 1007.
(59) Chemtob, S. M.; Nickerson, R. D.; Morris, R. V.; Agresti, D. G.; Catalano, J. G. Oxidative Alteration of Ferrous Smectites and Implications for the Redox Evolution of Early Mars. *J. Geophys. Res.: Planets* **2017**, *122*, 2469−2488.
(60) Redhammer, G. J.; Roth, G. Single-Crystal Structure Refinements and Crystal Chemistry of Synthetic Trioctahedral Micas KM3(Al3+,Si4+)4O10(OH)2, Where M = Ni2+, Mg2+, Co2+, Fe2+, or Al3+. *Am. Mineral.* **2002**, *87*, 1464−1476.
(61) Zabinsky, S. I.; Rehr, J. J.; Ankudinov, A.; Albers, R. C.; Eller, M. J. Multiple-Scattering Calculations of x-Ray-Absorption Spectra. *Phys. Rev. B: Condens. Matter Mater. Phys.* **1994**, *52*, 15−1995.
(62) Tyanova, S.; Temu, T.; Cox, J. The MaxQuant Computational Platform for Mass Spectrometry-Based Shotgun. *Proteomics* **2016**, *11*, 2301−2319.
(63) Tyanova, S.; Temu, T.; Sinitcyn, P.; Carlson, A.; Hein, M. Y.; Geiger, T.; Mann, M.; Cox, J. The Perseus Computational Platform for Comprehensive Analysis of (Prote)Omics Data. *Nat. Methods* **2016**, *13*, 731−740.
(64) Han, X.; Tomaszewski, E. J.; Sorwat, J.; Pan, Y.; Kappler, A.; Byrne, J. M. Oxidation of Green Rust by Anoxygenic Phototrophic Fe(II)-Oxidising Bacteria. *Geochem. Perspectives Lett.* **2020**, 52−57.
(65) Duckworth, O. W.; Martin, S. T. Role of Molecular Oxygen in the Dissolution of Siderite and Rhodochrosite. *Geochim. Cosmochim. Acta* **2004**, *68*, 607−621.
(66) Pankow, J. F.; Morgan, J. J. Dissolution of Tetragonal Ferrous Sulfide (Mackinawite) in Anoxic Aqueous Systems. 2. Implications for the Cycling of Iron, Sulfur, and Trace Metals. *Environ. Sci. Technol.* **1980**, *14*, 183−186.
(67) Ribeiro, F. R.; Fabris, J. D.; Kostka, J. E.; Komadel, P.; Stucki, J. W. Comparisons of Structural Iron Reduction in Smectites by Bacteria and Dithionite: II. A Variable-Temperature Mössbauer Spectroscopic Study of Garfield Nontronite. *Pure Appl. Chem.* **2009**, *81*, 1499−1509.
(68) Zhou, Nanqing.; Luther, G. W.; Chan, C. S. Ligand Effects on Biotic and Abiotic Fe(II) Oxidation by the Microaerophile *Sideroxydans Lithotrophicus*. *Environ. Sci. Technol.* **2021**, *55*, 9362−9371.
(69) McAllister, S. M.; Moore, R. M.; Gartman, A.; Luther, G. W.; Emerson, D.; Chan, C. S. The Fe(II)-Oxidizing Zetaproteobacteria:

https://doi.org/10.1021/acs.est.2c05142
Environ. Sci. Technol. XXXX, XXX, XXX−XXX

Historical, Ecological and Genomic Perspectives. *FEMS Microbiol. Ecol.* **2019**, *95*, No. fiz015.
(70) Noor, N.; Thompson, A. Localized Alteration of Ferrihydrite Natural Organic Matter Coprecipitates Following Reaction with Fe(II. *Soil Sci. Soc. Am. J.* **2022**, *86*, 253−263.
(71) Hartshorne, R. S.; Reardon, C. L.; Ross, D.; Nuester, J.; Clarke, T. A.; Gates, A. J.; Mills, P. C.; Fredrickson, J. K.; Zachara, J. M.; Shi, L.; Beliaev, A. S.; Marshall, M. J.; Tien, M.; Brantley, S.; Butt, J. N.; Richardson, D. J. Characterization of an Electron Conduit between Bacteria and the Extracellular Environment. *Proc. Natl. Acad. Sci. U.S.A.* **2009**, *106*, 22169−22174.
(72) Dong, H.; Jaisi, D. P.; Kim, J.; Zhang, G. Microbe-Clay Mineral Interactions. *Am. Mineral.* **2009**, *94*, 1505−1519.
(73) Pentráková, L.; Su, K.; Pentrák, M.; Stucki, J. W. A Review of Microbial Redox Interactions with Structural Fe in Clay Minerals. *Clay Miner.* **2013**, *48*, 543−560.
(74) Hernandez, M. E.; Newman, D. K. Extracellular Electron Transfer. *Cell. Mol. Life Sci.* **2001**, *58*, 1562−1571.
(75) Marsili, E.; Baron, D. B.; Shikhare, I. D.; Coursolle, D.; Gralnick, J. A.; Bond, D. R. Shewanella Secretes Flavins That Mediate Extracellular Electron Transfer. *Proc. Natl. Acad. Sci. U.S.A.* **2008**, *105*, 3968−3973.
(76) Weber, K. A.; Achenbach, La.; Coates, J. D. Microorganisms Pumping Iron: Anaerobic Microbial Iron Oxidation and Reduction. *Nat. Rev. Microbiol.* **2006**, *4*, 752−764.
(77) Keffer, J. L.; McAllister, S. M.; Garber, A. I.; Hallahan, B. J.; Sutherland, M. C.; Rozovsky, S.; Chan, C. S. Iron Oxidation by a Fused Cytochrome-Porin Common to Diverse Iron-Oxidizing Bacteria. *mBio* **2021**, *12*, No. e01074-21.
(78) White, G. F.; Edwards, M. J.; Gomez-Perez, L.; Richardson, D. J.; Butt, J. N.; Clarke, T. A. Mechanisms of Bacterial Extracellular Electron Exchange. *Adv. Microb. Physiol.* **2016**, *68*, 87−138.
(79) Jaisi, D. P.; Dong, H.; Plymale, A. E.; Fredrickson, J. K.; Zachara, J. M.; Heald, S.; Liu, C. Reduction and Long-Term Immobilization of Technetium by Fe(II) Associated with Clay Mineral Nontronite. *Chem. Geol.* **2009**, *264*, 127−138.
(80) Liao, W.; Ye, Z.; Yuan, S.; Cai, Q.; Tong, M.; Qian, A.; Cheng, D. Effect of Coexisting Fe(III) (Oxyhydr)Oxides on Cr(VI) Reduction by Fe(II)-Bearing Clay Minerals. *Environ. Sci. Technol.* **2019**, *53*, 13767−13775.
(81) Neumann, A.; Wu, L.; Li, W.; Beard, B. L.; Johnson, C. M.; Rosso, K. M.; Frierdich, A. J.; Scherer, M. M. Atom Exchange between Aqueous Fe(II) and Structural Fe in Clay Minerals. *Environ. Sci. Technol.* **2015**, *49*, 2786−2795.
(82) Gorski, C. A.; Klüpfel, L.; Voegelin, A.; Sander, M.; Hofstetter, T. B. Redox Properties of Structural Fe in Clay Minerals. 2. Electrochemical and Spectroscopic Characterization of Electron Transfer Irreversibility in Ferruginous Smectite, SWa-1. *Environ. Sci. Technol.* **2012**, *46*, 9369−9377.
(83) Gorski, C. A.; Klüpfel, L. E.; Voegelin, A.; Sander, M.; Hofstetter, T. B. Redox Properties of Structural Fe in Clay Minerals: 3. Relationships between Smectite Redox and Structural Properties. *Environ. Sci. Technol.* **2013**, *47*, 13477−13485.
(84) Zhang, G.; Kim, J.; Dong, H.; Sommer, A. J. Microbial Effects in Promoting the Smectite to Illite Reaction: Role of Organic Matter Intercalated in the Interlayer. *Am. Mineral.* **2007**, *92*, 1401−1410.
(85) Kim, J.-W.; Furukawa, Y.; Dong, H.; Newell, S. W. The Effect of Microbial Fe(III) Reduction on Smectite Flocculation. *Clays Clay Miner.* **2005**, *53*, 572−579.
(86) Zuo, H.; Huang, L.; Chu, R. K.; Tolic, N.; Washton, N.; Zhu, Z.; Edelmann, R. E.; Elagamy, S.; Sommer, A.; Luan, F.; Zeng, Q.; Chen, Y.; Hu, D.; Zhan, D.; Hu, J.; Dong, H. Reduction of Structural Fe(III) in Nontronite by Humic Substances in the Absence and Presence of Shewanella Putrefaciens and Accompanying Secondary Mineralization. *Am. Mineral.* **2021**, *106*, 1957−1970.
(87) Neumann, A.; Hofstetter, T. B.; Skarpeli-Liati, M.; Schwarzenbach, R. P. Reduction of Polychlorinated Ethanes and Carbon Tetrachloride by Structural Fe(II) in Smectites. *Environ. Sci. Technol.* **2009**, *43*, 4082−4089.
(88) Benzine, J.; Shelobolina, E.; Xiong, M. Y.; Kennedy, D. W.; McKinley, J. P.; Lin, X.; Roden, E. E. Fe-Phyllosilicate Redox Cycling Organisms from a Redox Transition Zone in Hanford 300 Area Sediments. *Front. Microbiol.* **2013**, *4*, 388.
(89) Converse, B. J.; McKinley, J. P.; Resch, C. T.; Roden, E. E. Microbial Mineral Colonization across a Subsurface Redox Transition Zone. *Front. Microbiol.* **2015**, *6*, 858.
(90) Baker, I. R.; Conley, B. E.; Gralnick, J. A.; Girguis, P. R. Evidence for Horizontal and Vertical Transmission of Mtr-Mediated Extracellular Electron Transfer among the Bacteria. *mBio* **2022**, *13*, No. e02904-21.

https://doi.org/10.1021/acs.est.2c05142
Environ. Sci. Technol. XXXX, XXX, XXX−XXX